Geoscience Frontiers 9 (2018) 1309–1323

HOSTED BY

Contents lists available at ScienceDirect

China University of Geosciences (Beijing)

Geoscience Frontiers

journal homepage: www.elsevier.com/locate/gsf

Research Paper

Fluid-induced high-temperature metasomatism at Rundvågshetta in the Lützow-Holm Complex, East Antarctica: Implications for the role of brine during granulite formation

Kazuki Takahashi [a], Toshiaki Tsunogae [a,b,*], Emmanuel Nwachukwu Ugwuonah [a,c]

[a] Graduate School of Life and Environmental Sciences, University of Tsukuba, Ibaraki 305-8572, Japan
[b] Department of Geology, University of Johannesburg, Auckland Park 2006, South Africa
[c] Department of Geology, Chukwuemeka Odumegwu Ojukwu University, Uli, Nigeria

ARTICLE INFO

Article history:
Received 1 August 2017
Received in revised form
7 November 2017
Accepted 21 November 2017
Available online 8 December 2017

Keywords:
High-temperature metasomatism
Brine
Phase equilibrium modeling
Fluid inclusion
Gondwana
Lützow-Holm Complex

ABSTRACT

We report new petrological, phase equilibria modeling, and fluid inclusion data for pelitic and mafic granulites from Rundvågshetta in the highest-grade region of the Neoproterozoic Lützow-Holm Complex (LHC), East Antarctica, and provide unequivocal evidence for fluid-rock interaction and high-temperature metasomatism in the presence of brine fluid. The studied locality is composed dominantly of well-foliated pelitic granulite (K-feldspar + quartz + sillimanite + garnet + ilmenite) with foliation-parallel bands and/or layers of mafic granulite (plagioclase + orthopyroxene + garnet + ilmenite + quartz + biotite). The boundary between the two lithologies is defined by thin (about 1–20 cm in thick) garnet-rich layers with a common mineral assemblage of garnet + plagioclase + quartz + ilmenite + biotite ± orthopyroxene. Systematic increase of grossular and decrease of pyrope contents in garnet as well as decreasing Mg/(Fe + Mg) ratio of biotite from the pelitic granulite to garnet-rich rock and mafic granulite suggest that the garnet-rich layer was formed by metasomatic interaction between the two granulite lithologies. Phase equilibria modeling in the system NCKFMASHTO demonstrates that the metasomatism took place at 850–860 °C, which is slightly lower than the peak metamorphism of this region, and the modal abundance of garnet is the highest along the metapelite–metabasite boundary (up to 40%), which is consistent with the field and thin section observations. The occurrence of brine (7.0–10.9 wt.% $NaCl_{eq}$ for ice melting or 25.1–25.5 wt.% $NaCl_{eq}$ for hydrohalite melting) fluid inclusions as a primary phase trapped within plagioclase in the garnet-rich layer and the occurrence of Cl-rich biotite (Cl = 0.22–0.60 wt.%) in the metasomatic rock compared to that in pelitic (0.15–0.24 wt.%) and mafic (0.06–0.13 wt.%) granulites suggest infiltration of brine fluid could have given rise to the high-temperature metasomatism. The fluid might have been derived from external sources possibly related to the formation of major suture zones formed during the Gondwana amalgamation.

1. Introduction

Fluids associated with granulite-facies metamorphism have been regarded to be low in H_2O activity because of their roles in stabilizing orthopyroxene-bearing anhydrous mineral assemblages (e.g., Newton et al., 1998; Santosh and Omori, 2008). Previous petrological studies on granulites worldwide argued that CO_2-bearing fluid probably played an important role for lowering H_2O activity in the rocks (e.g., Newton et al., 1980; Santosh et al., 1990; Touret and Huizenga, 2011, 2012). Although there are some arguments that fluid-absent metamorphism related to dehydration melting can also be a possible mechanism to form granulites (e.g., Le Breton and Thompson, 1988; Clemens, 1990; Stevens and Clemens, 1993), the widespread occurrences of metamorphic fluids trapped as primary or pseudosecondary inclusions in various granulite-facies minerals confirm that at least some fluids must have been present during high-grade metamorphism (e.g., Newton et al., 1980; Touret, 1985; Santosh et al., 1990; Tsunogae et al., 2002; Ohyama et al., 2008a; Touret and Huizenga, 2012) and create a

* Corresponding author. Graduate School of Life and Environmental Sciences, University of Tsukuba, Ibaraki 305-8572, Japan.
E-mail address: tsunogae@geol.tsukuba.ac.jp (T. Tsunogae).
Peer-review under responsibility of China University of Geosciences (Beijing).

https://doi.org/10.1016/j.gsf.2017.11.010

natural curiosity to investigate the roles of these fluids in the overall metamorphism of the host rocks.

Recent investigations of lower crustal fluid demonstrated that high-salinity brine could have also played a major role on the formation of granulite-facies rocks (e.g., Harlov, 2012; Higashino et al., 2013; Tsunogae and van Reenen, 2014; Kawakami et al., 2017). One of the characters of brine is its important role on the solubility and transportation of elements in high-grade metamorphic rocks (Newton and Manning, 2007, 2008) as well as lowering H_2O activity. Tsunogae and van Reenen (2014) reported the occurrence of high-salinity brine fluid inclusions in metasomatic alteration zone along a crustal-scale shear zone in the Limpopo Complex, South Africa, and inferred transportation of K, Ca, and Mg by brine infiltration and formation of garnet–sillimanite–mesoperthite gneiss from enderbite at a temperature of 900 °C. Higashino et al. (2013) evaluated regional chlorine content of biotite within metasediments in the Sør Rondane Mountains, East Antarctica, and suggested the effect of Cl-bearing fluid or melt during granulite formation. Kawakami et al. (2017) argued the infiltration of chlorine-rich aqueous fluid along major tectonic boundaries in the Sør Rondane Mountains. Once such deep-seated brine fluids are generated, they will probably percolate along mineral grain boundaries, transfer dissolved mineral components, give rise to continuous alteration, and form metasomatic zones along fluid pathways. Brine fluids in the lower crust are thus considered to have played a major role in geochemical differentiation and material circulation, as well as lowering the H_2O activity of the fluid phase to form granulites (Santosh et al., 2009; Aranovich et al., 2013).

In this study, we present new petrological data for a metasomatic zone between pelitic and mafic granulites from the Lützow-Holm Complex (LHC) of East Antarctica (Fig. 1), and discuss evidences for high-temperature (~850 °C) metasomatism related to the activity of high-salinity aqueous fluids. The LHC is an example of regionally metamorphosed amphibolite- to granulite-facies terrane (e.g., Shiraishi and Yoshida, 1987; Shiraishi et al., 1989) formed during the latest Neoproterozoic collisional event related to the final phase of amalgamation of continental fragments during Gondwana assembly (ca. 600–550 Ma, e.g., Shiraishi et al., 2008 and references therein). Rundvågshetta region corresponds to the highest-grade area of the complex where ultrahigh-temperature (UHT) peak *P–T* conditions of 1040 °C and 13–15 kbar have been reported (e.g., Kawasaki et al., 2011). Although numerous petrological studies have been published from the LHC, most of them focused on the determination of peak metamorphic conditions and evaluation of *P–T* evolution of some unique UHT rocks (e.g., Motoyoshi and Ishikawa, 1997; Yoshimura et al., 2008; Kawasaki et al., 2011). Detailed investigations on the role of fluid associated with granulite formation in the complex are still limited except for some fluid inclusion studies from different localities (e.g., Santosh and Yoshida, 1992; Satish-Kumar et al., 2006; Takahashi and Tsunogae, 2017). This study is thus the first attempt to evaluate fluid-rock interaction during high-grade metamorphism of the LHC by performing microthermometric measurements of fluid inclusions and applying phase equilibrium modeling technique in the system Na_2O–CaO–K_2O–FeO–MgO–Al_2O_3–SiO_2–H_2O–TiO_2–Fe_2O_3 (NCKFMASHTO) using THERMOCALC 3.40 (e.g., Powell and Holland, 1988). The results of this study have important implications for fluid-rock interaction and the role of infiltrating reactive fluids during ~550 Ma peak or near-peak metamorphism in the root zone of the latest Neoproterozoic collisional orogeny.

2. Geological setting

2.1. Geology of the Lützow-Holm Complex

The Lützow-Holm Complex exposed along the Prince Harald and Prince Olav Coasts of East Antarctica (Fig. 1) is composed of felsic to mafic orthogneisses (biotite–hornblende gneiss, charnockite, dioritic gneiss, mafic granulite, and amphibolite), metasediments (pelitic and psammitic gneiss, quartzite, and marble), metagabbroic rocks (garnet–clinopyroxene granulite), and later-stage intrusive rocks (metagranite and pegmatite). Available petrological studies of metasedimentary and metabasic rocks of the LHC indicate an increase in metamorphic grade from amphibolite-facies in the northeast to granulite-facies in the southwest of the complex (e.g., Hiroi et al., 1991) with the highest-grade rocks of *T* ~1040 °C exposed at Rundvågshetta (e.g., Motoyoshi et al., 1985; Kawasaki et al., 1993, 2011; Motoyoshi and Ishikawa, 1997; Fraser et al., 2000; Yoshimura et al., 2008). Nogi et al. (2013) traced

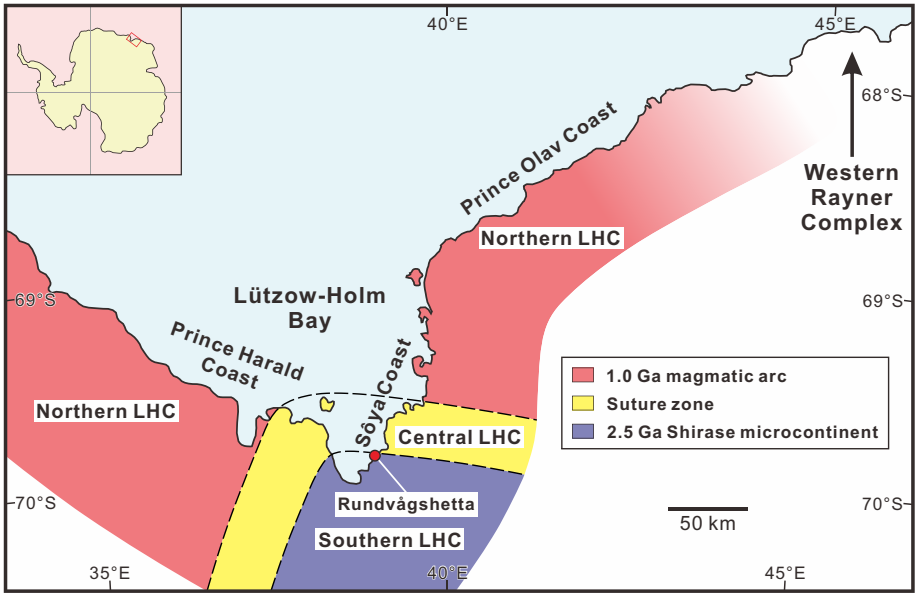

Figure 1. A generalized geological framework of the Lützow-Holm Complex with the locality of Rundvågshetta (after Toyoshima, 2017; Takahashi et al., 2018).

several geological structures within the LHC based on their geophysical data, and subdivided the complex into four discrete blocks possibly bounded by NE–SW-trending right lateral strike-slip faults. They also evaluated the presence of crustal gaps along the boundaries of the amphibolite-facies zone, the transitional zone, and the granulite-facies zone of the complex, and inferred the transitional zone as a remnant of the Western Rayner Complex. Iwamura et al. (2013) estimated peak UHT conditions for garnet-bearing mafic granulite from Akarui Point in the amphibolite–granulite transitional zone as 5–6 kbar and 900–920 °C, which are higher than the conditions from surrounding exposures, and argued that the LHC might be separated into several crustal blocks by shear zones as inferred from available geophysical data of Nogi et al. (2013).

Available geochemical, geochronological, and geophysical data suggest that the LHC can be subdivided into three blocks (Fig. 1); the Neoarchean (ca. 2.5 Ga) arc magmatic unit in the southern LHC (Shirase microcontinent), the Neoproterozoic (ca. 1.0 Ga) arc magmatic unit in the northern LHC, and the metasedimentary unit in the central LHC (e.g., Shiraishi et al., 2008; Suda et al., 2008; Tsunogae et al., 2014, 2015, 2016; Kazami et al., 2016; Takahashi et al., 2018; Takamura et al., 2018). Takahashi et al. (2018) argued that the metasedimentary unit in the central LHC corresponds to a suture zone formed by collision of ca. 2.5 Ga unit (Shirase microcontinent) and ca. 1.0 Ga unit (northern Lützow-Holm–Vijayan Complex) during the Late Neoproterozoic–Cambrian (600–550 Ma) high-grade metamorphic event (e.g., Shiraishi et al., 1994, 2003, 2008; Asami et al., 1997; Hokada and Motoyoshi, 2006; Dunkley et al., 2014; Tsunogae et al., 2014, 2015, 2016; Kawakami et al., 2016; Takamura et al., 2018).

2.2. Geology of Rundvågshetta

Rundvågshetta in the southwestern part of the LHC is one of the well-studied exposures in terms of metamorphic *P–T* conditions (Motoyoshi et al., 1985, 1986; Kawasaki et al., 1993, 2011; Motoyoshi and Ishikawa, 1997; Fraser et al., 2000; Yoshimura et al., 2008). The dominant lithologies of Rundvågshetta are charnockite, pelitic granulite, mafic to ultramafic granulites, and intrusive pegmatites (Motoyoshi et al., 1986). Charnockite is the most dominant lithology particularly in the central and southern parts, while pelitic granulites occur in the northern and central parts of the exposure. Mafic and ultramafic granulites are often present as boudins and pods within charnockite and pelitic granulite. The granulites have ESE–WNW to E–W foliation dipping mostly toward south and sometimes toward north. The pelitic granulites contain some unique mineral assemblages such as spinel + quartz (Motoyoshi et al., 1985; Kawasaki et al., 2011), orthopyroxene + sillimanite + quartz (Kawasaki et al., 1993; Motoyoshi and Ishikawa, 1997; Fraser et al., 2000), sapphirine + quartz (Yoshimura et al., 2008), and osumilite-bearing assemblages (Kawasaki et al., 2011), which are diagnostic of peak UHT metamorphism. Metamorphic *P–T* conditions recorded in Rundvågshetta granulites have been estimated to be >900 °C by Kawasaki et al. (1993) and Motoyoshi and Ishikawa (1997), based on geothermometry and mineral stability in pelitic granulites. Yoshimura et al. (2008) inferred the peak *P–T* condition of 1000–1100 °C from ternary-feldspar and Al-in-orthopyroxene geothermometers as well as the occurrence of sapphirine + quartz inclusions in a garnet porphyroblast in garnet–sillimanite–orthopyroxene granulite. Kawasaki et al. (2011) examined osumilite- and spinel + quartz-bearing granulites from the area and estimated the peak condition of 1040 °C at 13–15 kbar, which was followed by retrograde stages of 950 °C at 8 kbar and 830 °C at 6.1 kbar along a clockwise *P–T* path. In contrast, Tsunogae et al. (2014) estimated *P–T* conditions for charnockites from Rundvågshetta and adjacent Vesleknausen as 750–890 °C, and inferred that the UHT event is a local phenomenon recorded in dry Mg–Al-rich pelitic rocks, whereas metamorphic temperature of adjacent orthogneisses was probably buffered by breakdown or dehydration-melting reactions of biotite/hornblende to form pyroxenes in charnockite.

Fraser et al. (2000) obtained zircon U–Pb age of 517 ± 9 Ma from a syn-deformational leucosome as the timing of peak metamorphism. Shiraishi et al. (2003) reported similar Cambrian SHRIMP zircon age of 521 ± 9 Ma for garnet–biotite gneiss from Rundvågshetta as the time of peak metamorphism. Shiraishi et al. (2008) obtained 2.53 Ga Sm–Nd depleted mantle model age of garnet–biotite–sillimanite pelitic gneiss, and Dunkley et al. (2014) reported Neoarchean (ca. 2.5 Ga) magmatic ages based on SHRIMP U–Pb geochronology from the region. A slightly older metamorphic age of 555 ± 3.5 Ma was obtained by Tsunogae et al. (2016) for felsic orthogneiss from the central part of the region based on LA-ICP-MS zircon U–Pb geochronology. They also obtained zircon Lu–Hf isotope data of felsic orthogneiss with the crustal residence ages (T^{C}_{DM}) ranging from 3881 Ma to 3783 Ma with an average of 3837 Ma, suggesting that the protolith felsic magma might have been sourced from reworked Paleoarchean crust. K/Ar and $^{40}Ar/^{39}Ar$ ages of ca. 500 Ma from hornblende and biotite probably mark the last thermal event of this region at about 350–300 °C (Fraser et al., 2000).

3. Field occurrence of lithological units

The samples discussed in this study were collected from a thick metasedimentary unit in the northern part of Rundvågshetta during the field geological survey of Lützow-Holm Bay area undertaken by the 52nd Japanese Antarctic Research Expedition (JARE-52) in 2010–2011. The unit is composed dominantly of highly-foliated leucocratic garnet–sillimanite (pelitic) gneiss and intercalated mafic granulite with boudins and lenses of less-foliated garnet–sapphirine-bearing Mg–Al-rich rock, biotite–sillimanite–garnet rock, and sillimanite–quartz rock.

The studied locality (69°54′11.5″S, 39°03′08.9″E) is composed dominantly of leucocratic (felsic) gneiss with continuous and semi-continuous layers, bands, and boudins of melanocratic (mafic) rocks (see Fig. 2a). The general trend of foliation is ESE–WNW to E–W with a dip direction in the south to southwest, which is consistent with the major foliation of the central LHC along the Sôya and Prince Harald Coasts (Shiraishi et al., 1989). The mafic layers measure from less than 1 cm to about 1 m thick.

On a closer observation (see Fig. 2b), the leucocratic gneiss which we shall be referring to as the 'pelitic granulite' unit ('PG' in Fig. 2b; sample Ts11011802B) is revealed as a coarse-grained dominantly leucocratic to mesocratic rock which has strong alignment of minerals in a preferred direction. The unit is further differentiated into different bands and domains of mesocratic and leucocratic rocks showing different amounts of coarse- to medium-grained reddish-brown garnet. The modal abundance of the garnets is higher in the mesocratic bands (the less feldspathic and grayish bands). Other mineral constituents of this unit include feldspars (K-feldspar and minor plagioclase), quartz and subordinate biotite and sillimanite.

The melanocratic bands in the study area form a distinct lithology of unique mineralogy and texture. This unit which we shall be referring to as the 'mafic granulite' ('MG' in Fig. 2b; sample Ts11011802E) is medium grained and semi-equigranular. The mineral constituents are not obvious in the field, but grains of reddish-brown garnet can be seen to be almost uniformly distributed within the rock comprising about 15%–20% of the unit.

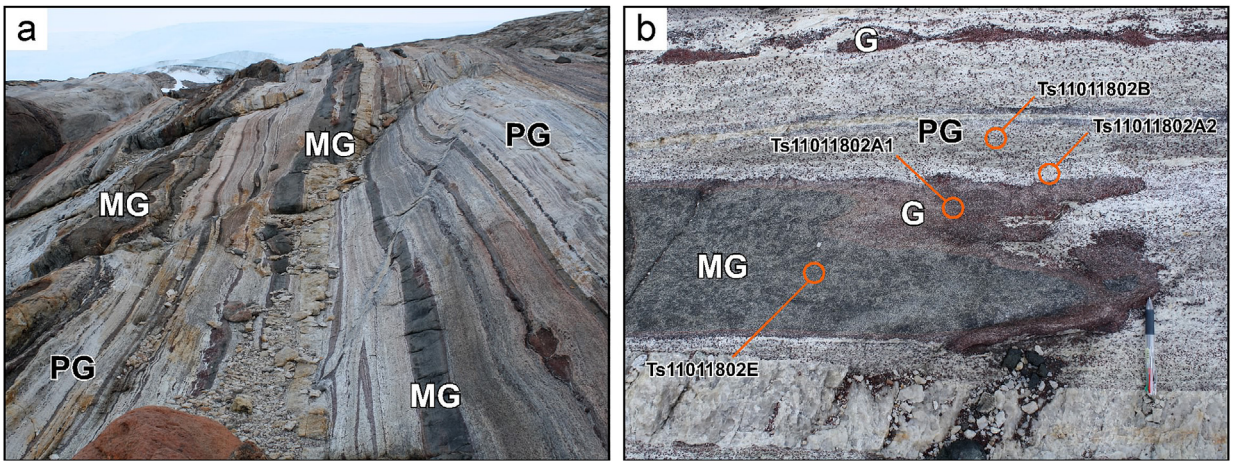

Figure 2. Field photographs showing occurrences and textures of garnet-rich metasomatic rocks and associated granulites in Rundvågshetta. (a) Highly foliated layers of mafic granulite (MG) intercalated with pelitic granulite (PG). (b) Garnet-rich metasomatic rocks (G) between pelitic and mafic granulites. Approximate sampling points are also shown in the figure.

Bounding all the bands of the mafic unit like envelops, are rims of densely garnetiferous mineralogy measuring variously in thickness about 1–2 cm along the length of the mafic bands to about 15–20 cm at the broken ends of the bands (Fig. 2b). Within this densely garnetiferous envelope which we shall be referring to as the 'garnet-rich metasomatic rock' ('G' in Fig. 2b; sample Ts11011802A1), it seems that all other mafic minerals have been changed to garnet and the reddish-brown color of the garnet has become the color of the sub-unit. All small-sized boudins of the mafic granulites have been changed or recrystallized into garnet-dominated domains so that some chains of mafic boudins have become entirely chains of monomineralic garnet domains. The boundary between the garnet-rich rock and the host pelitic granulite is defined by leucocratic layers with lower modal abundance of garnet (sample Ts11011802A2).

4. Petrography

The salient petrographic features of the rocks examined in this study are summarized below. Representative thin-section photomicrographs are shown in Fig. 3. Mineral name abbreviations are after Kretz (1983).

4.1. Pelitic gneiss (sample Ts11011802B)

This is a coarse-grained and porphyroblastic rock with alignment of minerals in a preferred direction (Fig. 3a). It is composed of K-feldspar (25%–35%), garnet (15%–25%), quartz (15%–25%), and sillimanite (15%–25%). Accessory minerals are biotite, spinel, zircon, monazite, ilmenite, and rutile. Perthitic K-feldspar (0.8–4.5 mm) and quartz (0.2–6.4 mm) are subidioblastic to xenoblastic and elongated, and have tiny sillimanite needles as inclusions. Garnet (0.8–4.5 mm) is poikiloblastic and contains many inclusions, such as quartz, biotite, monazite, and spinel. Biotite is only found as rare inclusions in garnet. Sillimanite (0.1–3.3 mm) occurs as bundles, rods, and needles. Sillimanite bundles dominate the sillimanite population and help to define the direction of foliation of the rock. Some sillimanite grains have inclusions of spinel and ilmenite.

4.2. Mafic granulite (sample Ts11011802E)

This rock is composed of plagioclase (20%–30%), orthopyroxene (15%–25%), biotite (5%–15%), garnet (5%–15%), quartz (5%–10%), Fe–Ti oxide (mainly ilmenite; 5%–10%), and apatite (2%–4%) (Fig. 3b). Plagioclase (0.1–2.3 mm) and quartz (0.1–1.9 mm) dominate the matrix population. Orthopyroxene is fine- to medium-grained (0.1–1.5 mm), xenoblastic, and scattered in the matrix. Biotite is also fine- to medium-grained (0.1–1.2 mm), and occurs in the matrix as flakes. Garnet (0.1–2.8 mm) is porphyroblastic, and partly surrounded by fine-grained orthopyroxene + plagioclase symplectite (Fig. 3b), suggesting the progress of the following continuous reaction (1):

$$\mathrm{Grt} + \mathrm{Qtz} \Rightarrow \mathrm{Opx} + \mathrm{Pl} \quad (1)$$

Similar reaction textures have been reported from many high-grade terranes worldwide (Harley, 1989), probably suggesting near-isothermal decompression or decompressional cooling after the peak metamorphism. Fe–Ti oxide occurs as fine- to medium-grained (0.1–1.8 mm) minerals, and apatite occurs as fine-grained (0.1–0.5 mm) minerals in the matrix.

4.3. Garnet-rich metasomatic rock

This rock type between the pelitic and mafic granulite is characterized by high modal abundance of garnet (up to 85%) in the matrix of quartz, feldspars, and biotite. Sample Ts11011802A1 is composed of garnet (35%–45%), biotite (15%–25%), plagioclase (10%–20%), quartz (5%–15%), and opaque minerals (mainly ilmenite and rare pyrite; 2%–7%) with accessory apatite, zircon, and monazite (Fig. 3c). Garnet (0.1–2.1 mm) grows as clusters or mosaics (up to 85%). It is idioblastic to subidioblastic, and smaller-sized grains are filling up spaces between larger grains. Individual coarse-grained garnet is separated by microcrystalline plagioclases and blades of biotites away from the large clusters. The size and number of garnet crystals decrease toward the contact with mafic granulite (sample Ts11011802E). Plagioclase (0.1–1.6 mm) and quartz (0.1–1.3 mm) are xenoblastic, and fill up spaces between larger grains of garnet. Biotite is fine- to medium-grained (0.1–3.0 mm) and scattered in the matrix. It also occurs as biotite-rich folia which is characterized by a dense population of biotite blades (up to 70%) in strong defined alignment with garnet, quartz, and plagioclase. Apatite also occurs as fine-grained (0.1–0.3 mm) minerals in the matrix.

Sample Ts11011802A2 is more leucocratic and coarse-grained than sample Ts11011802A1, and is composed of garnet (25%–35%), plagioclase (25%–35%), biotite (10%–20%), quartz (5%–15%),

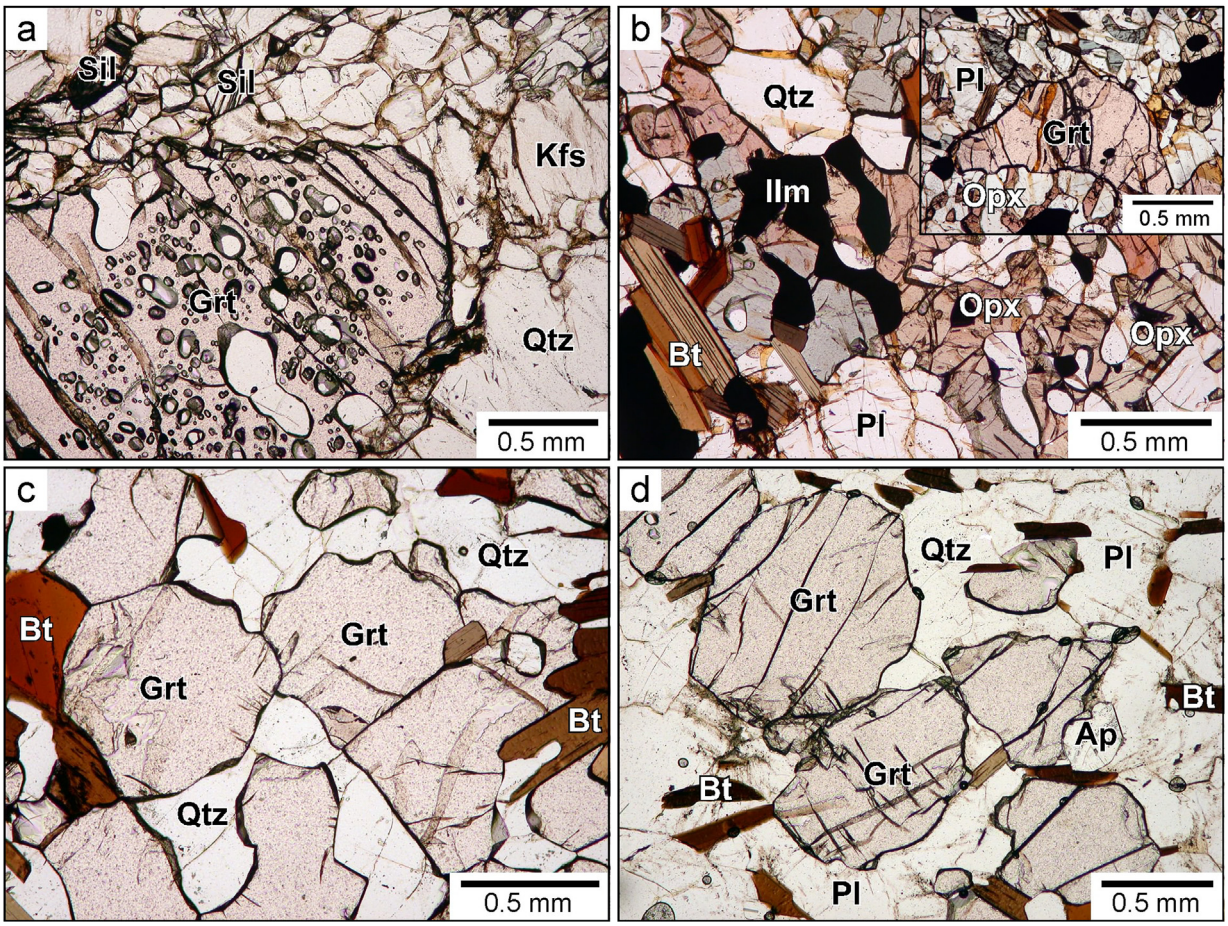

Figure 3. Photomicrographs showing representative textures and mineral assemblages of samples discussed in this study. (a) Poikiloblastic garnet in the matrix of quartz, K-feldspar, and elongated sillimanite in pelitic granulite (sample Ts11011802B). (b) Subidioblastic orthopyroxene + biotite + plagioclase + ilmenite assemblage in mafic granulite (sample Ts11011802E). (c) Highly garnet-rich metasomatic rock (sample Ts11011802A1). (d) Idioblastic garnet in the matrix of quartz, plagioclase, and biotite in garnet-rich metasomatic rock (sample Ts11011802A2).

and apatite (2%–7%), with accessory ilmenite, rutile, spinel, zircon, and monazite (Fig. 3d), which is essentially the same mineralogy as Ts11011802A1 except for the lower modal abundance of garnet and the occurrence of rare orthopyroxene. Garnet (0.1–3.3 mm) forms the porphyroblast and has little to no inclusions except rare spinel grains, although fine- to medium-grained xenoblastic or elongated garnets also occur in the matrix. Biotite occurs as fine- to medium-grained (0.1–1.5 mm), and xenoblastic to subidioblastic minerals. Plagioclase (0.1–1.4 mm) and quartz (0.1–2.1 mm) are xenoblastic and equigranular, and fill the matrix of garnet and biotite. Apatite also occurs as fine-grained (0.1–0.3 mm) minerals in the matrix. Rare orthopyroxene (less than 0.1 vol.%) is fine-grained (0.1–0.5 mm), and xenoblastic to subidioblastic.

5. Mineral chemistry

Mineral chemical analyses were carried out using an electron microprobe (JEOL JXA8530F) at the Chemical Analysis Division of the Research Facility Center for Science and Technology, the University of Tsukuba. The analyses were performed under conditions of 15 kV accelerating voltage and 10 nA sample current, and the data were regressed using an oxide-ZAF correction program supplied by JEOL. Representative mineral chemistry data are summarized in Tables 1–4.

5.1. Biotite

Biotite composition varies depending on lithology (Table 1). The biotite in mafic granulite (sample Ts11011802E) shows intermediate mole Mg/(Fe + Mg) ratio (= X_{Mg}) of 0.50–0.58, whereas that in metasomatic rock (samples Ts11011802A1 and Ts11011802A2) and pelitic granulite (sample Ts11011802B) is slightly enriched in Mg as X_{Mg} = 0.59–0.74, 0.60–0.70, and 0.62–0.66, respectively (Fig. 4a,b). In contrast, TiO_2 content of biotite does not show any obvious variation as 4.87–7.03 wt.% (mafic granulite), 4.04–5.78 wt.% (metasomatic rock; Ts11011802A1), 3.72–5.69 wt.% (metasomatic rock; Ts11011802A2), and 5.55–7.43 wt.% (pelitic granulite).

The biotite in the metasomatic rock shows higher chlorine contents of Cl/(F + Cl + OH) = 0.03–0.05 [Ts11011802A1] and 0.03–0.08 [Ts11011802A2] than that in pelitic granulite (0.02–0.03 [Ts11011802B]) and mafic granulite (0.01–0.02 [Ts11011802E]) (Fig. 4a,c). That in the orthopyroxene-bearing portion of the metasomatic rock (Ts11011802A2) shows the highest chlorine content of Cl/(F + Cl + OH) and the lowest TiO_2 contents of 0.07–0.08 and 3.72–4.41 wt.%, respectively.

Fluorine content of biotite in metasomatic rocks (F/(F + Cl + OH) = 0.03–0.13 [Ts11011802A1] and 0.05–0.14 [Ts11011802A2]) is relatively higher than that in mafic granulite (0.00–0.08 [Ts11011802E]) and pelitic granulite (0.03–0.08 [Ts11011802B]) (Fig. 4b). It shows a positive correlation with X_{Mg}

(Fig. 4b), suggesting Fe^{2+}–F avoidance in biotite (e.g., Rosenberg and Foit, 1977). In contrast, there is no obvious correlation between Cl and X_{Mg} in biotite (Fig. 4a). Both, Cl and F in biotite show a negative correlation with TiO_2 (Fig. 4c,d). Fig. 4e suggests a slight positive correlation between Cl and F contents in biotite.

5.2. Apatite

Apatite in the examined samples is enriched in F than Cl (Table 2). That in mafic granulite shows higher fluorine content (F/(F + Cl + OH) = 0.40–0.49 [Ts11011802E]) than that in metasomatic rocks (0.32–0.40 [Ts11011802A1] and 0.29–0.39 [Ts11011802A2]) (see Fig. 4f). In contrast, apatite in the metasomatic rocks shows higher Cl content (Cl/(F + Cl + OH) = 0.09–0.14 [Ts11011802A1] and 0.10–0.17 [Ts11011802A2]) than that in mafic granulite (0.01–0.02 [Ts11011802E]) (Fig. 4f). Particularly, apatite in the orthopyroxene-bearing portion of sample Ts11011802A2 shows the highest chlorine content of Cl/(F + Cl + OH) = 0.16–0.17 which is consistent with the case of biotite. There is a slight negative correlation between F and Cl contents of the apatites (Fig. 4f).

5.3. Garnet

Garnet in the samples is essentially almandine-rich with varying pyrope, grossular, and spessartine contents depending on lithology (Table 3). The garnet in mafic granulite (Ts11011802E) shows higher grossular and spessartine and lower pyrope contents ($Alm_{58–64}Prp_{19–21}Grs_{12–21}Sps_{3–4}$) than that in pelitic granulite ($Alm_{61–63}Prp_{33–35}Grs_3Sps_1$ [Ts11011802B]). Garnet in the metasomatic rock shows intermediate compositions of $Alm_{57–64}Prp_{29–37}Grs_{5–8}Sps_{1–2}$ (Ts11011802A1) and $Alm_{59–67}Prp_{26–35}Grs_{5–7}Sps_{1–2}$ (Ts11011802A2). Compositional zoning is observed for garnet in mafic granulite (Ts11011802E) showing slightly grossular-rich core ($Alm_{58–59}Prp_{19}Grs_{18–21}Sps_{3–4}$) and almandine-rich rim ($Alm_{63–64}Prp_{19–21}Grs_{12–13}Sps_4$), whereas garnets in the other lithologies do not show any significant chemical zonation.

5.4. Orthopyroxene

The orthopyroxene composition varies depending on lithology. The orthopyroxene in the metasomatic rock (Ts11011802A2) shows higher X_{Mg} of 0.61–0.62 than that in mafic granulite (X_{Mg} = 0.47–0.59; Ts11011802E). X_{Mg} of orthopyroxene increases from the central part of the mafic granulite (X_{Mg} = 0.47–0.53) toward the contact with the metasomatic rock (X_{Mg} = 0.58–0.59).

5.5. Feldspars

Plagioclase in the samples shows a notable compositional variation depending on lithology. The plagioclase in mafic granulite (Ts11011802E) shows the highest anorthite content of $An_{82–89}$ probably reflecting high CaO content of the rock, whereas that in the garnet-rich metasomatic rocks (Ts11011802A1 and

Table 1
Representative electron microprobe analyses of biotite. See Fig. 2 for abbreviations of lithologies.

Mineral name	Biotite (O = 22)				
Sample No.	Ts11011802B (PG)	Ts11011802A2 (G)		Ts11011802A1 (G)	Ts11011802E (MG)
Remarks		Opx-absent	Opx-bearing		
SiO_2	35.25	35.86	36.79	36.26	34.49
Al_2O_3	16.04	15.40	14.43	15.57	14.54
TiO_2	7.43	5.07	4.27	5.03	5.26
Cr_2O_3	0.12	0.06	0.03	0.01	0.17
FeO[a]	13.17	14.32	14.13	14.43	17.35
MnO	0.00	0.01	0.10	0.03	0.03
NiO	0.15	0.12	0.11	0.00	0.07
MgO	12.74	13.22	15.18	13.81	11.98
CaO	0.01	0.00	0.01	0.00	0.02
Na_2O	0.29	0.02	0.00	0.07	0.02
K_2O	8.93	9.53	9.53	8.67	8.64
F	0.20	0.35	0.46	0.32	0.16
= O (F)	−0.08	−0.15	−0.19	−0.13	−0.07
Cl	0.22	0.37	0.60	0.32	0.11
= O (Cl)	−0.05	−0.08	−0.13	−0.07	−0.02
Total	94.40	94.10	95.29	94.31	92.72
Si	5.303	5.460	5.535	5.469	5.391
Al	2.843	2.763	2.559	2.766	2.678
Ti	0.840	0.580	0.483	0.571	0.618
Cr	0.015	0.008	0.003	0.001	0.020
Fe	1.656	1.823	1.778	1.819	2.267
Mn	0.000	0.001	0.012	0.004	0.003
Ni	0.018	0.014	0.013	0.000	0.009
Mg	2.854	2.998	3.403	3.103	2.789
Ca	0.001	0.000	0.001	0.000	0.003
Na	0.084	0.006	0.000	0.021	0.005
K	1.713	1.851	1.828	1.668	1.723
Total	15.327	15.503	15.615	15.422	15.506
F	0.095	0.167	0.220	0.152	0.077
Cl	0.056	0.095	0.152	0.081	0.028
Mg/(Fe + Mg)	0.63	0.62	0.66	0.63	0.55
F/(F + Cl + OH)	0.05	0.08	0.11	0.08	0.04
Cl/(F + Cl + OH)	0.03	0.05	0.08	0.04	0.01

[a] Total Fe as FeO.

Table 2
Representative electron microprobe analyses of apatite.

Mineral name	Apatite (O = 12.5)			
Sample No.	Ts11011802A2 (G)		Ts11011802A1 (G)	Ts11011802E (MG)
Remarks	Opx-absent	Opx-bearing		
SiO_2	0.06	0.11	0.13	0.19
FeO[a]	1.09	0.41	0.45	0.34
MnO	0.10	0.06	0.09	0.05
MgO	0.18	0.04	0.03	0.04
CaO	53.21	54.14	53.97	53.45
P_2O_5	42.56	41.70	42.39	41.89
F	2.42	2.38	2.53	3.45
= O (F)	−1.02	−1.00	−1.07	−1.45
Cl	1.71	2.26	1.73	0.25
= O (Cl)	−0.38	−0.51	−0.39	−0.06
Total	99.93	99.57	99.86	98.16
Si	0.005	0.009	0.011	0.016
Fe	0.077	0.029	0.032	0.024
Mn	0.007	0.004	0.006	0.004
Mg	0.023	0.004	0.003	0.005
Ca	4.799	4.936	4.875	4.880
P	3.033	3.004	3.025	3.022
Total	7.945	7.986	7.952	7.951
F	0.645	0.639	0.675	0.930
Cl	0.243	0.326	0.247	0.036
F/(F + Cl + OH)	0.32	0.32	0.34	0.46
Cl/(F + Cl + OH)	0.12	0.16	0.12	0.02

[a] Total Fe as FeO.

Ts11011802A2) is enriched in albite component as $An_{43–65}$ and $An_{40–58}$, respectively. Rim of plagioclase ($An_{56–65}$) in the plagioclase-rich portion of garnet-rich sample Ts11011802A1 is slightly enriched in anorthite content than core ($An_{43–54}$), possibly suggesting extraction of Na from the mineral into fluids during metasomatism or transportation of Ca from adjacent mafic granulite. The plagioclase in the orthopyroxene-bearing portion of sample Ts11011802A2 is also slightly enriched in anorthite content ($An_{54–58}$) than that in the orthopyroxene-absent portion ($An_{40–50}$).

Table 3
Representative electron microprobe analyses of garnet.

Mineral name	Garnet (O = 12)							
Sample No.	Ts11011802B (PG)		Ts11011802A2 (G)		Ts11011802A1 (G)		Ts11011802E (MG)	
Remarks	Core	Rim	Core	Rim	Core	Rim	Core	Rim
SiO_2	39.04	38.87	38.93	38.67	38.30	38.63	37.23	36.95
Al_2O_3	21.98	21.70	21.85	21.53	21.95	21.76	20.24	20.29
TiO_2	0.00	0.06	0.03	0.00	0.01	0.05	0.08	0.05
Cr_2O_3	0.00	0.06	0.00	0.05	0.05	0.08	0.06	0.03
FeO[a]	28.62	29.01	27.67	28.26	27.58	28.19	27.04	29.76
MnO	0.38	0.31	0.72	0.68	0.79	0.93	1.35	1.94
MgO	9.04	8.94	8.64	8.78	8.25	8.10	5.02	4.91
CaO	1.14	1.16	2.35	1.85	2.82	2.29	7.52	4.87
Na_2O	0.04	0.02	0.00	0.00	0.02	0.00	0.00	0.03
K_2O	0.01	0.01	0.00	0.01	0.01	0.01	0.01	0.00
Total	100.25	100.14	100.19	99.82	99.78	100.02	98.53	98.82
Si	3.005	3.002	3.001	2.999	2.974	2.996	2.985	2.977
Al	1.994	1.975	1.985	1.967	2.008	1.988	1.912	1.926
Ti	0.000	0.003	0.001	0.000	0.001	0.003	0.005	0.003
Cr	0.000	0.004	0.000	0.003	0.003	0.005	0.004	0.002
Fe	1.841	1.873	1.783	1.833	1.790	1.827	1.812	2.004
Mn	0.025	0.020	0.047	0.045	0.052	0.061	0.091	0.132
Mg	1.036	1.028	0.992	1.014	0.954	0.936	0.599	0.589
Ca	0.094	0.096	0.194	0.154	0.235	0.190	0.645	0.420
Na	0.006	0.003	0.000	0.000	0.003	0.000	0.000	0.005
K	0.001	0.000	0.000	0.001	0.001	0.001	0.001	0.000
Total	8.002	8.007	8.005	8.016	8.021	8.006	8.053	8.058
Mg/(Fe + Mg)	0.36	0.35	0.36	0.36	0.35	0.34	0.25	0.23
Alm	61.45	62.07	59.12	60.18	59.06	60.63	57.57	63.72
Prp	34.57	34.07	32.90	33.31	31.47	31.04	19.03	18.72
Grs	3.14	3.19	6.42	5.05	7.74	6.30	20.50	13.35
Sps	0.83	0.67	1.56	1.47	1.72	2.02	2.90	4.21

[a] Total Fe as FeO.

Table 4
Representative electron microprobe analyses of orthopyroxene and feldspars.

Mineral name	Orthopyroxene (O = 6)				Plagioclase (O = 8)						K-feldspar (O = 8)
Sample No.	Ts11011802A2 (G)	Ts11011802E (MG)			Ts11011802A2 (G)		Ts11011802A1 (G)		Ts11011802E (MG)		Ts11011802B (PG)
Remarks		Contact	Central part	Symplectite	Opx-absent	Opx-bearing	Core	Rim	Matrix	Symplectite	
SiO_2	50.03	49.11	50.78	49.06	57.17	53.81	54.76	52.83	46.91	44.71	64.25
Al_2O_3	4.33	3.54	1.95	1.75	26.83	29.00	28.45	29.62	34.18	33.97	18.76
TiO_2	0.12	0.07	0.07	0.01	0.01	0.03	0.00	0.00	0.03	0.00	0.01
Cr_2O_3	0.01	0.06	0.09	0.08	0.08	0.00	0.00	0.00	0.00	0.04	0.00
FeO[a]	22.84	25.50	29.88	27.83	0.06	0.11	0.11	0.10	0.25	0.37	0.00
MnO	0.17	0.36	0.77	0.51	0.01	0.04	0.06	0.00	0.02	0.03	0.00
MgO	20.91	19.38	16.08	17.70	0.00	0.00	0.00	0.00	0.01	0.00	0.00
CaO	0.11	0.17	0.35	0.37	9.29	11.55	10.43	12.03	17.74	17.04	0.20
Na_2O	0.01	0.00	0.01	0.01	6.35	5.03	5.65	4.72	1.33	1.46	2.33
K_2O	0.01	0.00	0.01	0.00	0.23	0.22	0.12	0.10	0.06	0.06	13.30
Total	98.54	98.18	99.97	97.32	100.01	99.78	99.58	99.40	100.52	97.68	98.84
Si	1.895	1.897	1.963	1.939	2.567	2.440	2.480	2.407	2.146	2.110	2.978
Al	0.193	0.161	0.089	0.082	1.420	1.549	1.518	1.590	1.843	1.889	1.024
Ti	0.003	0.002	0.002	0.000	0.000	0.001	0.000	0.000	0.001	0.000	0.000
Cr	0.000	0.002	0.003	0.002	0.003	0.000	0.000	0.000	0.000	0.001	0.000
Fe	0.723	0.823	0.966	0.920	0.002	0.004	0.004	0.004	0.009	0.015	0.000
Mn	0.006	0.012	0.025	0.017	0.000	0.002	0.002	0.000	0.001	0.001	0.000
Mg	1.180	1.115	0.926	1.042	0.000	0.000	0.000	0.000	0.000	0.000	0.000
Ca	0.004	0.007	0.014	0.015	0.447	0.561	0.506	0.587	0.869	0.861	0.010
Na	0.000	0.000	0.001	0.000	0.552	0.442	0.495	0.417	0.118	0.134	0.209
K	0.000	0.000	0.001	0.000	0.013	0.013	0.007	0.006	0.003	0.004	0.786
Total	4.005	4.020	3.990	4.019	5.004	5.012	5.012	5.010	4.992	5.014	5.008
Mg/(Fe + Mg)	0.62	0.58	0.49	0.53	Ab 54.58	43.53	49.15	41.28	11.91	13.38	20.83
					Or 1.28	1.25	0.68	0.59	0.35	0.37	78.19
					An 44.14	55.23	50.17	58.13	87.74	86.25	0.98

[a] Total Fe as FeO.

The K-feldspar in pelitic granulite (Ts11011802B) shows orthoclase-rich compositions of $Or_{75–85}$. Compositional zoning is not obvious.

6. Geothermobarometry

Metamorphic *P–T* conditions recorded in this lithological unit were estimated based on conventional geothermobarometry to infer the condition of the formation of the garnet-rich metasomatic rocks. The garnet–orthopyroxene–plagioclase–quartz geothermobarometry was applied to porphyroblastic garnet and orthopyroxene associated with plagioclase and quartz in mafic granulite sample Ts11011802E. The estimated temperature range for the garnet–orthopyroxene pairs are 810–860 °C at 7–8 kbar based on the method of Bhattacharya et al. (1991). Application of the method of Lee and Ganguly (1988) gave slightly higher temperatures of 860–920 °C. Metamorphic pressure was calculated using garnet–orthopyroxene–plagioclase–quartz assemblages in the same sample based on the experimental calibration of Perkins and Newton (1981). The estimated results are 6.7–7.3 kbar at 800–900 °C. Application of the method of Moecher et al. (1988), which adopted revised thermodynamic and experimental data, yielded a pressure range of 7.7–9.3 kbar, which is slightly higher than the results of Perkins and Newton (1981). We therefore infer that *P–T* conditions recorded in the mafic granulite is 810–920 °C and 6.7–9.3 kbar, which are slightly lower than the peak condition of this region (1040 °C at 13–15 kbar; Kawasaki et al., 2011).

7. Fluid inclusions

7.1. Fluid inclusion petrography

Fluid inclusions trapped in various coarse-grained minerals in the garnet-rich metasomatic rock (sample Ts11011802A1) were studied in order to characterize the fluid associated with the metasomatism. The occurrence, shape, size, and phase category of the fluid inclusions were observed using doubly polished thin wafers of about 180 microns in thickness under a petrological microscope following the techniques outlined by Roedder (1984), Touret (2001), and Van den Kerkhof and Hein (2001). Fluid inclusions are dominantly trapped in plagioclase grains in the sample. The inclusions are very small (less than 18 μm in length), and show rectangular to irregular shape, commonly reflecting the crystal character of the host plagioclase (Fig. 5). Their occurrences as isolated inclusions away from the grain margin or any visible healed cracks suggest that the inclusions are 'primary' inclusions trapped during the growth of the host mineral (e.g., Roedder, 1984). No obvious solid phase was found within the cavity of the inclusions. As the plagioclase occurs as a coarse-grained and subidioblastic mineral closely associated with porphyroblastic garnet, it is likely to have grown during metasomatism, suggesting that the fluids trapped within the primary inclusions could represent the fluid associated with the metasomatic event. Plagioclase and garnet grains in the sample also contain abundant secondary fluid inclusions that occur along healed fractures continuing to the edge of the host minerals ('S' in Fig. 5), suggesting that the inclusions were trapped during post-peak exhumation stage. However, they are too small for microthermometric study.

7.2. Microthermometry

Microthermometric measurements of the inclusions were performed with a Linkam heating/freezing system at the University of Tsukuba following the technique described in Tsunogae et al. (2002, 2008). Calibration of temperatures was undertaken with a synthetic standard material for H_2O and a natural internal standard (Santosh and Tsunogae, 2003; Tsunogae et al., 2008) for CO_2. The calibration was performed at 0 °C (triple point of pure H_2O), −56.6 °C (triple point of CO_2), and the critical point of pure H_2O with a density of 0.317 g/cm^3 (374.1 °C). Melting temperature

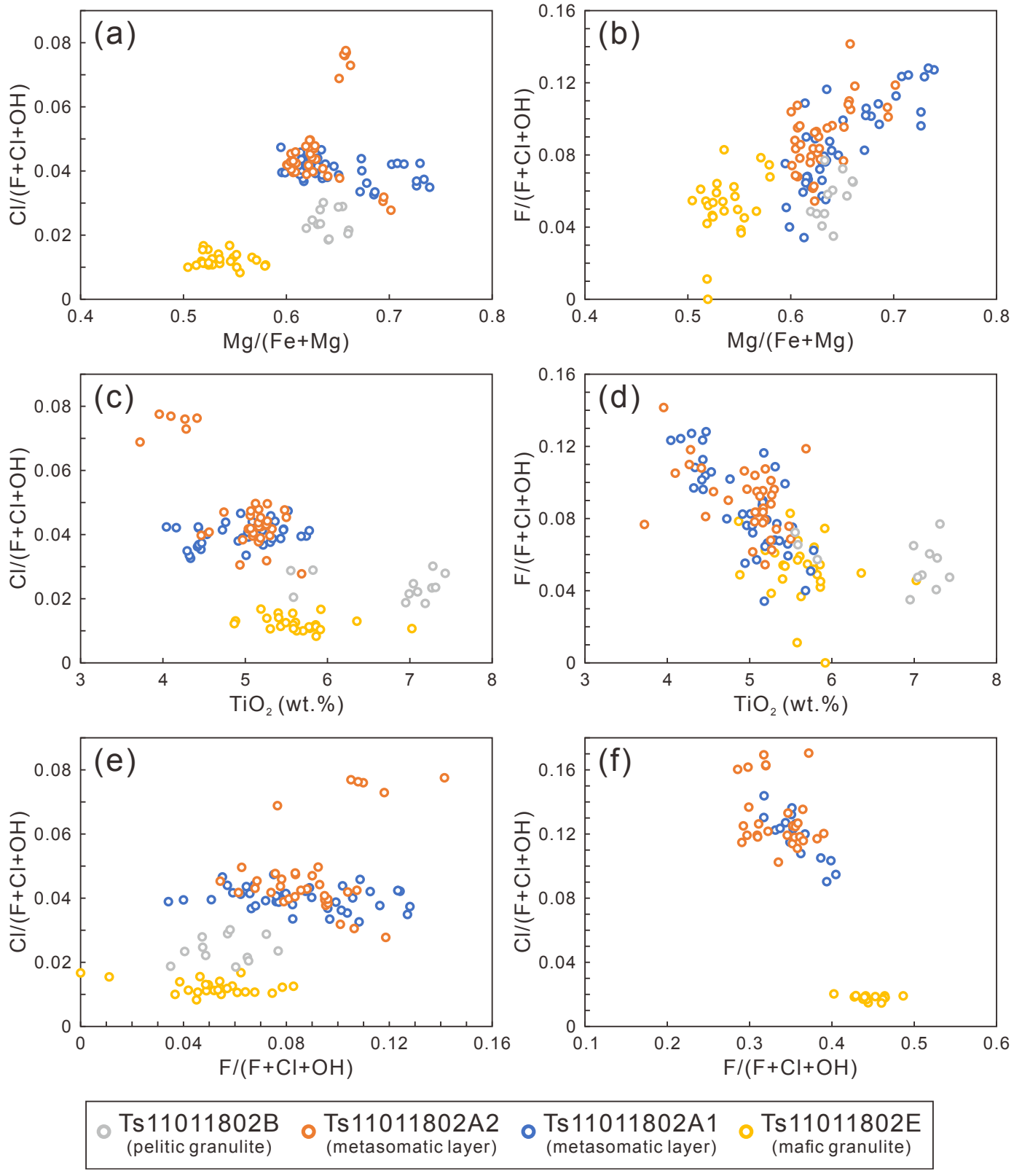

Figure 4. Compositional diagrams showing biotite and apatite chemistry. (a) Mg/(Fe + Mg) vs. Cl/(F + Cl + OH) diagram for biotite. (b) Mg/(Fe + Mg) vs. F/(F + Cl + OH) diagram for biotite. (c) TiO_2 vs. Cl/(F + Cl + OH) diagram for biotite. (d) TiO_2 vs. F/(F + Cl + OH) diagram for biotite. (e) F/(F + Cl + OH) vs. Cl/(F + Cl + OH) diagram for biotite. (f) F/(F + Cl + OH) vs. Cl/(F + Cl + OH) diagram for apatite.

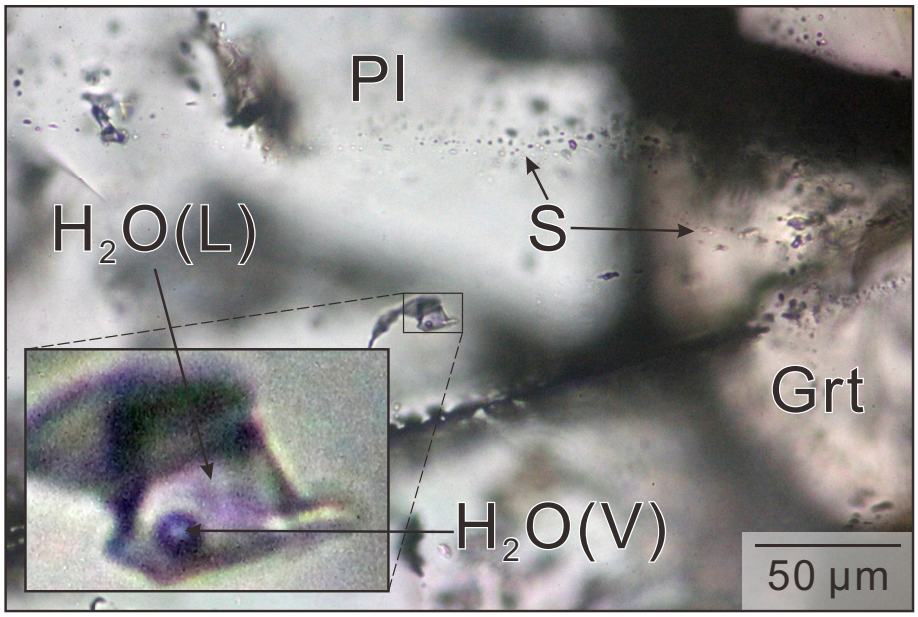

Figure 5. Photomicrograph of a representative aqueous fluid inclusion in garnet-rich metasomatic rock (sample Ts11011802A1). H_2O–vapor bubble (H_2O (V)) is surrounded by H_2O–liquid (H_2O (L)) in the inclusion. Its occurrence as an isolated inclusion away from the grain margins suggests a primary origin. 'S' indicates array of fine-grained secondary fluid inclusions.

(*Tm*) and homogenization temperature (*Th*) of two-phase (gas–vapor) inclusions were measured during the heating/cooling experiment. Heating rates of the samples were 1 °C/min for *Tm* and 5 °C/min for *Th*. Repeated microthermometric measurements indicate that the precision of microthermometric results reported in this study is within ±0.2 °C for *Tm* and ±0.5 °C for *Th*. Although we spent many days for searching primary fluid inclusions, we could obtain microthermometric data for only five fluid inclusions probably because aqueous fluid identified in this study is highly mobile due to its low wetting angle. The salinities, densities and isochores were calculated using the computer program "MacFlinCor" developed by Brown and Hagemann (1994) based on the equation and thermodynamic data of Bodnar and Vityk (1994).

Although we attempted to analyze both initial- and final-melting temperatures during freezing experiments, we failed to measure initial-melting temperatures because of very small size of the inclusions. Therefore, we could only obtain final-melting temperatures of solid phases for the five inclusions as −7.3 °C to −4.4 °C. All the aqueous inclusions homogenized into the liquid phase at *Th* = 134.6–363.3 °C.

In this study, we could not identify the solid phase (either ice or hydrohalite) because we have no access to Raman spectrometer. We therefore calculated salinities for both cases based on the *Tm* values as 7.0–10.9 wt.% $NaCl_{eq}$ (ice melting) or 25.1–25.5 wt.% $NaCl_{eq}$ (hydrohalite melting). The result implies that the trapped fluid is dominantly H_2O with salt. The densities of the inclusions are estimated based on the *Th* values as 0.70–1.00 g/cm^3 $NaCl_{eq}$ (ice) or 0.90–1.12 g/cm^3 $NaCl_{eq}$ (hydrohalite).

8. Phase equilibrium modeling

The metamorphic conditions and fluid-rock interaction during metasomatism have been investigated using temperature versus bulk-rock composition (T–X_{bulk}) pseudosections. The calculations were performed using THERMOCALC 3.40 (Powell and Holland, 1988; Holland and Powell, 1998, 2011) and the internally consistent thermodynamic dataset of Holland and Powell (1998, 2011; data set tc-ds62, file created February 2012). We neglected MnO in the modeling because of low concentrations. The pseudosection calculations were therefore performed in the chemical system Na_2O–CaO–K_2O–FeO–MgO–Al_2O_3–SiO_2–H_2O–TiO_2–Fe_2O_3 (NCKFMASHTO), which is probably the most suitable approximation to model the metabasite–metapelite association examined in this study. The phases considered in the modeling and the corresponding a–x models used are tonalitic melt (for metabasite) and clinoamphibole (Green et al., 2016), haplogranitic melt (for metapelite), orthopyroxene, garnet, and biotite (White et al., 2014), feldspars (Holland and Powell, 2003), and ilmenite–hematite (White et al., 2000). Quartz, rutile, and sillimanite are treated as pure phases. For the analysis, slabs of unaltered and relatively homogeneous parts of the examined rocks were used for thin-section preparation, and the counterparts of the same slabs were used for chemical analysis. Bulk-rock compositions for the rocks were determined by X-ray fluorescence spectroscopy at Activation Laboratories, Canada. The chemical compositions (in wt.%) are SiO_2 = 60.86, Al_2O_3 = 24.05, FeO = 7.80, Fe_2O_3 = 0.69, MgO = 2.02, CaO = 0.28, Na_2O = 0.61, K_2O = 3.81, TiO_2 = 0.86, FeO^T/MgO = 2.91 for pelitic granulite (sample Ts11011802B) and SiO_2 = 41.78, Al_2O_3 = 15.06, FeO = 15.30, Fe_2O_3 = 4.03, MgO = 6.50, CaO = 8.04, Na_2O = 0.46, K_2O = 0.43, TiO_2 = 5.93, FeO^T/MgO = 4.17 for mafic granulite (sample Ts11011802E). The mafic granulite sample contains ~1.14 wt.% P_2O_5, which is reflected in ~4 modal % of apatite. As we neglect P_2O_5 from the system, the CaO content equivalent to apatite should be extracted from the calculation. The corrected CaO content (6.54 wt.%) is adopted for the pseudosection calculation.

Several T–X_{bulk} pseudosections (not shown) were constructed using the compositional data of mafic and pelitic granulites with varying pressure conditions (5–10 kbar) and mole H_2O contents ($M(H_2O)$; 0.2–2.0 mol.%), which are based on common P and $M(H_2O)$ ranges of granulite-facies metamorphism (e.g., Harley, 1989; Endo et al., 2012, 2013). Calculated T–X_{bulk} pseudosections suggest that appropriate mineral assemblages in mafic and pelitic granulites occur at P = 7.5 kbar, which is consistent with the results of geothermobarometry, and $M(H_2O)$ = 0.5. Therefore, we adopted the P and $M(H_2O)$ values for T–X_{bulk} pseudosection calculations. The T–X_{bulk} pseudosection in Fig. 6 is useful for evaluating the

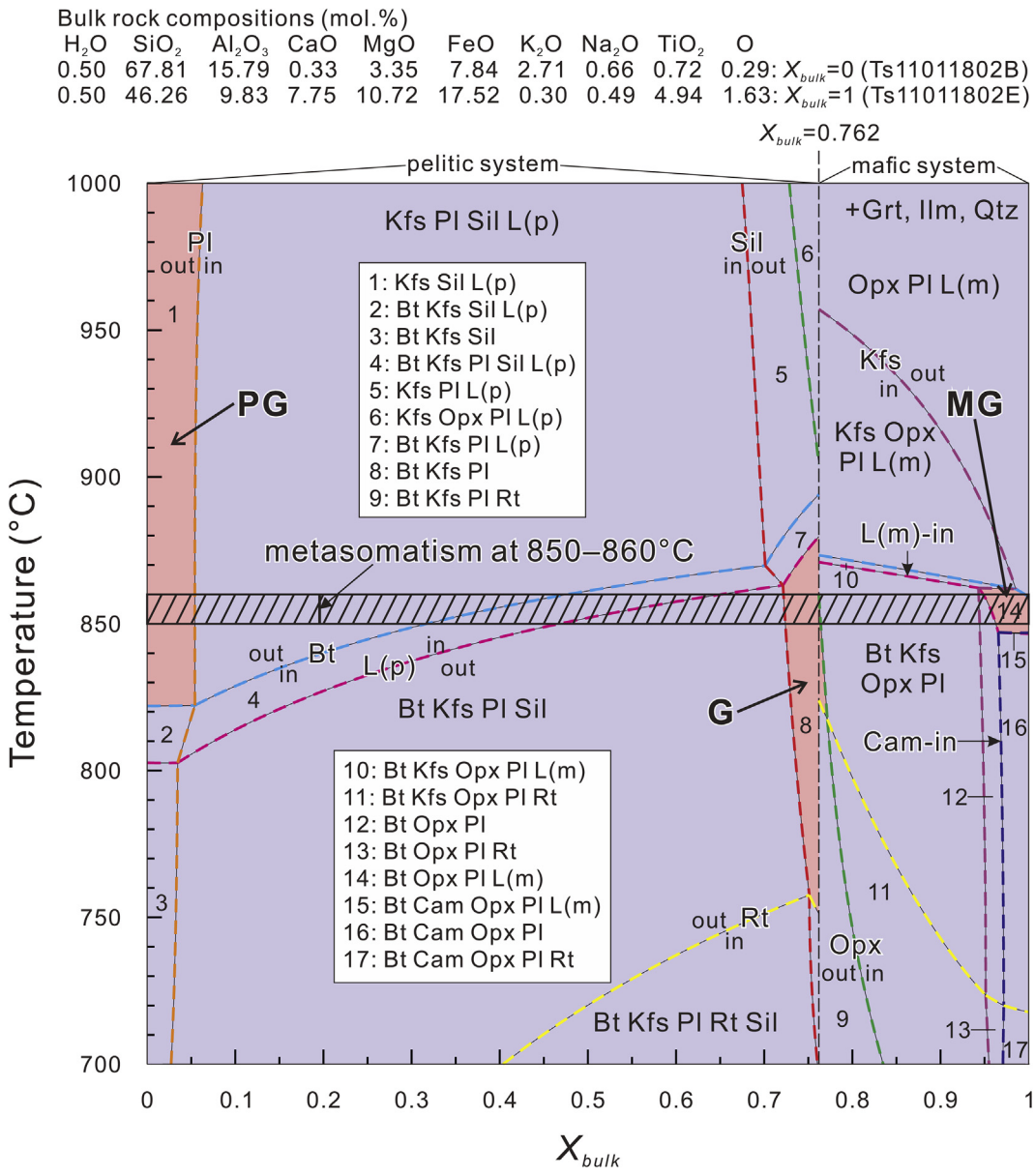

Figure 6. Temperature versus composition (T–X_{bulk}) pseudosection showing the stability relations of mineral assemblages in the samples discussed in this study. Shaded area implies the stability fields of mineral assemblages in pelitic granulite (PG), mafic granulite (MG), and garnet-rich metasomatic rock (G). See text for discussion. Mineral name abbreviations are after Kretz (1983). L(p): haplogranitic liquid for pelitic system. L(m): tonalitic liquid for mafic system.

effect of element mobility on the stability of the mineral assemblages preserved in host and metasomatized samples. The H_2O activities for the samples were calculated using THERMOCALC software at 850–860 °C (peak temperature) as 0.482–0.510 (pelitic granulite), 0.380–0.403 (pelitic portion of metasomatic rock), 0.281–0.299 (mafic portion of metasomatic rock), and 0.386–0.486 (mafic granulite), which is consistent with the inferred H_2O activity of granulite-facies rocks (0.3–0.6; e.g., Newton et al., 2014). Several petrological characters discussed in previous sections such as: (1) the occurrences of garnet-rich rock between pelitic and mafic granulites, (2) increasing grossular and decreasing pyrope contents in garnet from pelitic granulite to garnet-rich rock and mafic granulite as well as increasing Mg/(Fe + Mg) ratio of biotite from mafic granulite to garnet-rich rock and pelitic granulite, and (3) occurrence of brine fluid inclusions in garnet-rich rock suggest that the formation of the garnet-rich layer between the mafic and pelitic granulites is probably related to the progress of fluid-rock interaction and metasomatism. We therefore attempted to evaluate the variation of mineral assemblages using the bulk compositional data of the two rocks. The rock composition at $X_{bulk} = 0$ in Fig. 6 corresponds to that of pelitic granulite, while that at $X_{bulk} = 1$ corresponds to that of mafic granulite. Because we use both pelitic and mafic systems for the calculation of metasomatic mineral assemblages, we adopted haplogranitic liquid (L(p)) for pelitic system at $X_{bulk} < 0.762$ and tonalitic liquid (L(m)) for mafic system at $X_{bulk} > 0.762$ for the calculation including melt phase.

The calculated T–X_{bulk} pseudosection in Fig. 6 demonstrates that the apparent peak mineral assemblages in the pelitic granulite (Kfs + Qtz + Sil + Grt + Ilm + L(p)) and mafic granulite (Pl + Opx + Grt + Ilm + Qtz + Bt + L(m)) are stable at areas PG and MG, respectively, in the figure, and they can be both stable at 850–860 °C. At $X_{bulk} = 0.72$–0.77, Grt + Pl + Qtz + Ilm + Bt + Kfs becomes the stable assemblage (area G in Fig. 6), which is equivalent to the mineral assemblage of the metasomatic rocks

(Grt + Pl + Qtz + Ilm + Bt [Ts11011802A1 and Ts11011802A2]) except for the absence of K-feldspar in the samples, possibly because K-feldspar was hydrated during retrograde metamorphism forming retrograde biotites. The results of mineral equilibrium modeling are therefore consistent with the occurrence of natural mineral assemblages in the metasomatic rock, and confirmed that the metasomatism took place at granulite-facies condition (850–860 °C).

9. Discussion

9.1. High-temperature metasomatism in Rundvågshetta

This study reports the occurrence of garnet-rich metasomatic rocks between pelitic (Kfs + Qtz + Sil + Grt + Ilm ± inferred melt; sample Ts11011802B) and mafic (Pl + Opx + Grt + Ilm + Qtz + Bt ± inferred melt; sample Ts11011802E) granulites from a metasedimentary unit of Rundvågshetta in the Lützow-Holm Complex, East Antarctica, and argues a possible effect of high-temperature metasomatism induced by infiltration of brine fluid during high-grade metamorphism. The metasomatic rock contains granulite-facies mineral assemblages of Grt + Pl + Qtz + Ilm + Bt ± Opx with high modal abundance of garnet (about 40%–50% on average, and up to 85% in some domains). Whole-rock compositional data of the two host lithologies indicate that CaO and FeO are enriched in the mafic granulite, whereas Al_2O_3, MgO, and SiO_2 are enriched in the pelitic granulite. The dominant occurrence of almandine–pyrope–grossular-type garnet along their lithological boundary implies Ca and Fe were probably supplied from the mafic granulite, while Si, Al, and Mg were provided from the pelitic granulite for the formation of the garnet-rich layer. THERMOCALC software was employed to model the metasomatic process based on an available thermodynamic dataset and *a–x* models in the system NCKFMASHTO. T–X_{bulk} pseudosection in Fig. 6 suggests that peak mineral assemblages in pelitic and mafic granulites are stable at 850–860 °C at 7.5 kbar. Modal abundance of garnet increases with increasing X_{bulk} toward the highest modal garnet of 40% at around $X_{bulk} = 0.76$, and then decreases toward mafic granulite. The mineral assemblage of the garnet-rich layer (Grt + Pl + Qtz + Ilm + Bt + Kfs) occurs as a stable phase at $X_{bulk} = 0.72$–0.77 (area G in Fig. 6), which is consistent with the X_{bulk} value of the highest modal garnet, suggesting that the alteration process is probably controlled by element mobilization between the pelitic and mafic granulites. Orthopyroxene does not occur in the pseudosection calculation possibly because of its low modal abundance in the metasomatic rock (less than 0.1 modal %).

Such element mobilization during high-temperature metasomatism is also confirmed by the variation in mineral chemistry. For example, garnet shows increasing grossular and decreasing pyrope contents from the pelitic granulite ($Alm_{61–63}Prp_{33–35}Grs_3Sps_1$ [Ts11011802B]) toward the garnet-rich metasomatic rock ($Alm_{57–67}Prp_{26–37}Grs_{5–8}Sps_{1–2}$ [Ts11011802A1 and Ts11011802A2]) and mafic granulite ($Alm_{58–64}Prp_{19–21}Grs_{12–21}Sps_{3–4}$ [Ts11011802E]). Biotite shows increasing X_{Mg} from mafic granulite (0.50–0.58) toward the metasomatic rock (0.59–0.74) and pelitic granulite (0.62–0.66). These mineral chemical characters can be explained by metasomatic processes between pelitic and mafic granulites.

The P–T condition of the formation of metasomatic garnet-rich rock (850–860 °C at 7.5 kbar) is consistent with the condition obtained from garnet–orthopyroxene–plagioclase–quartz geothermobarometry of mafic granulite (810–920 °C and 6.7–9.3 kbar), but the temperature range is at least 100 °C lower than the inferred peak (1040 °C at 13–15 kbar) condition of Rundvågshetta obtained from spinel-bearing Mg–Al-rich granulites (Kawasaki et al., 2011), possibly suggesting that the metasomatism might have taken place during retrograde metamorphism. However, Tsunogae et al. (2014) estimated peak temperature for a charnockite from Rundvågshetta as 750–890 °C, which is comparable with the temperature of metasomatism, based on phase equilibrium modeling technique, and argued that UHT metamorphism is a local event recorded only in dry Mg–Al-rich pelitic rocks. This phenomenon is also discussed for UHT granulites from the Limpopo Complex in southern Africa (Tsunogae and van Reenen, 2011) and the Palghat-Cauvery suture zone in southern India (Nishimiya et al., 2010). In the examples, the UHT metamorphic conditions (~1000 °C), which were recorded only in Mg–Al-rich and K–Si-poor rocks, are systematically higher than the P–T conditions obtained from adjacent lithologies. We therefore infer that the metasomatism in Rundvågshetta probably took place during or slightly after the peak metamorphism.

9.2. Fluid-induced metasomatism

Although lithological associations of pelitic and mafic granulites have been commonly observed from other localities in the granulite-facies region of the LHC, and also from many high-grade terranes worldwide, the boundaries between the two lithologies are generally sharply defined without any metasomatic zones except minor concentrations of garnet along the boundary. In such examples, CO_2-bearing fluid inclusions trapped during peak of metamorphism have been commonly reported (e.g., Santosh and Yoshida, 1992; Tsunogae et al., 2002, 2008; Santosh and Tsunogae, 2003; Tsunogae and van Reenen, 2007; Ohyama et al., 2008a,b; Santosh et al., 2008, 2010; Tsunogae and Santosh, 2011; Takahashi and Tsunogae, 2017), suggesting that CO_2 was the dominant fluid component of granulite-facies metamorphism (e.g., Touret, 1985). In this study, we report the occurrence of aqueous fluid inclusions with final melting temperatures of −7.3 °C to −4.4 °C, which correspond to a salinity of 7.0–10.9 wt.% $NaCl_{eq}$, trapped as primary phase within plagioclase in the garnet-rich metasomatic rock. It has to be noted that Bodnar (2003) pointed out that "ice-melting" temperatures for aqueous fluid inclusions in many published reports may correspond to "hydrohalite-melting" temperatures because it is difficult to distinguish ice and hydrohalite during freezing experiments. Therefore, if the solid phase present during the freezing experiment corresponds to hydrohalite, although we are unable to identify the phase because laser-Raman spectrometer is not installed in our Linkam heating/freezing stage, salinity of our inclusions is estimated to be 25.1–25.5 wt.% $NaCl_{eq}$, based on which we infer that the fluid associated with the metasomatism is high-salinity brine. The metasomatic alteration and formation of garnet-rich layer in the present case are therefore probably related to infiltration of brine along the E–W trending lithological boundary between the pelitic and mafic granulites. This scenario is consistent with the evidence that biotite in the garnet-rich metasomatic rock shows significantly higher Cl content of 0.22–0.60 wt.% than that in pelitic granulite (Cl = 0.15–0.24 wt.%) and mafic granulite (Cl = 0.06–0.13 wt.%), suggesting that Cl was derived from salt dissolved in the hydrous fluids during the growth of the biotite in the metasomatized sample. Apatite in the metasomatic rock also shows higher Cl content of 1.26–2.34 wt.% than that in mafic granulite (Cl = 0.20–0.28 wt.%). The mineral chemistry data therefore suggest recrystallization/formation of biotite and apatite in the presence of high-salinity aqueous fluid. Such brine fluid could also play a major role in the transportation of elements during high-grade metamorphism. Newton and Manning (2007, 2008) reported increasing solubility of minerals (e.g.,

corundum, grossular) with increasing NaCl content of the interacting aqueous fluid. Therefore, it is inferred that interaction of rock-forming minerals with brine fluids played a critical role in the formation of garnet-rich metasomatic layers developed between pelitic and mafic granulites in Rundvågshetta. Lack of metasomatic zone in other granulite localities in the LHC could be explained by the lack of brine infiltration, which is supported by the dominant occurrence of CO_2-rich fluid inclusions.

It is also important to note that the biotite with the highest chlorine content of 0.54–0.60 wt.% in the orthopyroxene-bearing portion of garnet-rich metasomatic rock shows the highest fluorine content of ~0.59 wt.%. It is generally known that infiltration of low-H_2O activity ($a(H_2O)$) fluid enhances dehydration or dehydration melting of hydrosilicates (e.g., biotite, calcic amphibole) and formation of pyroxene-bearing anhydrous assemblages, and remaining hydrosilicates become enriched in F because fluorine tends to distribute in solid minerals rather than fluid or melt (e.g., Dooley and Patiño Douce, 1996; Tsunogae et al., 2003). The enrichment of F and Cl in biotite from the garnet-rich metasomatic rock therefore indicates the layer probably corresponds to a major fluid pathway.

The petrographical, bulk chemical, mineral chemical, microthermometric, and phase equilibria modeling data as well as the field occurrences of the examined samples discussed in this study therefore suggest element mobilization between the two lithologies and the formation of the garnet-rich metasomatic rocks through infiltration of brine from external sources along the lithological contacts.

9.3. Tectonic implications

Previous studies on chlorine-bearing biotites/amphiboles in granulite-facies rocks suggest that infiltration of externally-derived chlorine-bearing fluid is often associated with major shear zones or terrane boundaries. Tsunogae and van Reenen (2014) reported a metasomatic zone from the Petronella Shear Zone which corresponds to a major shear zone formed during the thrusting of the high-grade Limpopo Complex onto the low-grade Kaapvaal Craton at ca. 2.69 Ga. They inferred that dehydration of footwall greenstone belt lithology is a possible mechanism to generate Cl-bearing aqueous fluid, and the fluid infiltrated along the shear zone and metasomatized the hanging-rock side of the shear zone. Harlov et al. (1998) reported K-feldspar metasomatism induced by brine infiltration in charnockite from the Shevarory Hill Massif in southern India and the Bamble Sector in Norway. Recently, Higashino et al. (2013, 2015) reported chlorine-rich (Cl > 0.4 wt.%) biotites and amphiboles in pelitic and mafic gneisses from major tectonic boundaries or shear zones in Sør Rondane Mountains, East Antarctica, and inferred infiltration of Cl-bearing aqueous fluids along major crustal breaks.

Available geophysical data of Nogi et al. (2013) suggested that Rundvågshetta region is located along a boundary of negative and positive magnetic anomalies, based on which they defined a terrane boundary in this region. Takahashi et al. (2018) performed geochronological and geochemical investigations for orthogneisses from four localities in the LHC (Austhovde, Skallevikshalsem, Skallen, and Telen), and, together with available age data from the complex, inferred that metasedimentary units in the central LHC correspond to a major suture zone formed by collision of Neoarchean (ca. 2.5 Ga) microcontinent (Shirase microcontinent) and Neoproterozoic (ca. 1.0 Ga) magmatic arc (northern Lützow-Holm–Vijayan Complex). They argued that the metasedimentary unit in the northern part of Rundvågshetta corresponds to the southern margin of the suture zone, and the charnockite units in central and southern Rundvågshetta belong to the Neoarchean Shirase microcontinent (Fig. 1). The locality of the metasomatized rocks discussed in this study therefore may correspond to a major terrane boundary, along which chlorine-bearing fluid might have infiltrated during the latest Neoproterozoic high-grade metamorphism of the LHC associated with the final collision event during Gondwana amalgamation.

10. Conclusion

(1) Garnet-rich metasomatic rocks occur between pelitic and mafic granulites from a metasedimentary unit of Rundvågshetta in the Lützow-Holm Complex. The rock contains granulite-facies mineral assemblages of Grt + Pl + Qtz + Ilm + Bt ± Opx with high modal abundance of garnet. Systematic increase of grossular and decrease of pyrope contents in garnet as well as decreasing Mg/(Fe + Mg) ratio of biotite from the pelitic granulite to garnet-rich rock and mafic granulite suggest that the rock was formed by metasomatic interaction between the two granulite lithologies.

(2) Phase equilibria modeling in the system NCKFMASHTO demonstrates that peak mineral assemblages in pelitic and mafic granulites are stable at 850–860 °C at 7.5 kbar, which is consistent with the results of geothermobarometry. The *P–T* conditions are, however, slightly lower than the inferred peak metamorphism of this region, suggesting that the metasomatism took place during or slightly after the peak metamorphism. The modal abundance of garnet is the highest along the metapelite–metabasite boundary (up to 40%), which is consistent with the field and thin section observations.

(3) The occurrence of brine (7.0–10.9 wt.% $NaCl_{eq}$ (ice) or 25.1–25.5 wt.% $NaCl_{eq}$ (hydrohalite)) fluid inclusions as a primary phase trapped within plagioclase in the garnet-rich layer and the occurrence of Cl-rich biotite (0.22–0.60 wt.%) in the metasomatic rock compared to that in pelitic (0.15–0.24 wt.%) and mafic (0.06–0.13 wt.%) granulites suggest infiltration of brine fluid could have given rise to the high-temperature metasomatism. The fluid might have been derived from external sources possibly related to the formation of major suture zones formed during the Gondwana amalgamation.

Acknowledgments

We thank Profs. K. Shiraishi, Y. Motoyoshi, T. Kawasaki, Drs. T. Hokada, D.J. Dunkley, T. Miyamoto, M. Kato, and JARE-52 members for their support of geological field work. We also thank Akito Hiraga for supporting thin-section preparations and microprobe analysis. We also thank two anonymous reviewers for their constructive comments, and Prof. M. Santosh for his editorial comments and suggestions. Takahashi thanks his colleagues T. Koizumi, T. Endo, Y. Takamura, Y. Kuribara, M. Yano, C. Miyahara, Tang Li, and M. Amara for their support. Partial funding for this project was produced by a Grant-in-Aid for Scientific Research (B) from Japan Society for the Promotion of Science (JSPS) (No. 26302009) and by the NIPR General Collaboration Projects (No. 26-34) to Tsunogae.

References

Aranovich, L.Y., Newton, R.C., Manning, C.E., 2013. Brine-assisted anatexis: experimental melting in the system haplogranite–H_2O–NaCl–KCl at deep-crustal conditions. Earth and Planetary Science Letters 374, 111–120.

Asami, M., Suzuki, K., Adachi, M., 1997. Th, U and Pb analytical data and CHIME dating of monazites from metamorphic rocks of the Rayner, Lützow–Holm, Yamato–Belgica and Sør Rondane Complexes, East Antarctica. Proceedings of the NIPR Symposium on Antarctic Geosciences 10, 130–152.

Bhattacharya, A., Krishnakumar, K.R., Raith, M., Sen, S.K., 1991. An improved set of a–X parameters for Fe–Mg–Ca garnets and refinements of the

orthopyroxene–garnet thermometer and the orthopyroxene–garnet–plagioclase–quartz barometer. Journal of Petrology 32, 629–656.
Bodnar, R.J., 2003. Introduction to aqueous-electrolyte fluid inclusions. In: Samson, I., Anderson, A., Marshall, D. (Eds.), Fluid Inclusions: Analysis and Interpretation, Mineralogical Association of Canada, Short Course, vol. 32, pp. 81–99.
Bodnar, R.J., Vityk, M.O., 1994. Interpretation of microthermometric data for H_2O–NaCl fluid inclusions. In: De Vivo, B., Frezzotti, M.L. (Eds.), Fluid Inclusions in Minerals: Methods and Applications. Short Course of the International Mineralogical Association Working Group "Inclusions in Minerals". Virginia Polytechnic Institute Press, Blacksburg, pp. 117–130.
Brown, P.E., Hagemann, S.G., 1994. MacFlinCor: a computer program for fluid inclusion data reduction and manipulation. In: DeVivo, B., Frezzotti, M.L. (Eds.), Fluid Inclusions in Minerals: Methods and Applications. Short Course of the International Mineralogical Association Working Group "Inclusions in Minerals". Virginia Polytechnic Institute Press, Blacksburg, pp. 231–250.
Clemens, J.D., 1990. The granulite-granite connection. In: Vielzeuf, D., Vidal, P. (Eds.), Granulites and Crustal Differentiation. Kluwer, Dordrecht, The Netherlands, pp. 25–36.
Dooley, D.F., Patiño Douce, A.E., 1996. Fluid-absent melting of F-rich phlogopite + rutile + quartz. American Mineralogist 81, 202–212.
Dunkley, D.J., Shiraishi, K., Motoyoshi, Y., Tsunogae, T., Miyamoto, T., Hiroi, Y., Carson, C.J., 2014. Deconstructing the Lützow-Holm Complex with Zircon Geochronology. Abstract of 7th international SHRIMP workshop program, pp. 116–121.
Endo, T., Tsunogae, T., Santosh, M., Shaji, E., 2012. Phase equilibrium modeling of incipient charnockite formation in NCKFMASHTO and MnNCKFMASHTO systems: a case study from Rajapalaiyam, Madurai Block, southern India. Geoscience Frontiers 3, 801–811.
Endo, T., Tsunogae, T., Santosh, M., Shimizu, H., Shaji, E., 2013. Granulite formation in a Gondwana fragment: petrology and mineral equilibrium modeling of incipient charnockite from Mavadi, southern India. Mineralogy and Petrology 107, 727–738.
Fraser, G., McDougall, I., Ellis, D.J., Williams, I.S., 2000. Timing and rate of isothermal decompression in Pan-African granulites from Rundvågshetta, East Antarctica. Journal of Metamorphic Geology 18, 441–454.
Green, E.C.R., White, R.W., Diener, J.F.A., Powell, R., Holland, T.J.B., Palin, R.M., 2016. Activity–composition relations for the calculation of partial melting equilibria in metabasic rocks. Journal of Metamorphic Geology 34, 845–869.
Harley, S.L., 1989. The origin of granulites: a metamorphic perspective. Geological Magazine 126, 215–247.
Harlov, D.E., 2012. The potential role of fluids during regional granulite-facies dehydration in the lower crust. Geoscience Frontiers 3, 813–827.
Harlov, D.E., Hansen, E.C., Bigler, C., 1998. Petrologic evidence for K-feldspar metasomatism in granulite facies rocks. Chemical Geology 151, 373–386.
Higashino, F., Kawakami, T., Satish-Kumar, M., Ishikawa, M., Maki, K., Tsuchiya, N., Grantham, G.H., Hirata, T., 2013. Chlorine-rich fluid or melt activity during granulite facies metamorphism in the Late Proterozoic to Cambrian continental collision zone – an example from the Sør Rondane Mountains, East Antarctica. Precambrian Research 234, 229–246.
Higashino, F., Kawakami, T., Tsuchiya, N., Satish-Kumar, M., Ishikawa, M., Grantham, G.H., Sakata, S., Hattori, K., Hirata, T., 2015. Geochemical behavior of zirconium during Cl-rich aqueous fluid infiltration under upper amphibolite facies metamorphism—a case study from Brattnipene, Sør Rondane Mountains, East Antarctica. Journal of Mineralogical and Petrological Sciences 110, 166–178.
Hiroi, Y., Shiraishi, K., Motoyoshi, Y., 1991. Late Proterozoic paired metamorphic complexes in East Antarctica, with special reference to the tectonic significance of ultramafic rocks. In: Thomson, M.R.A., Crame, J.A., Thomson, J.W. (Eds.), Geological Evolution of Antarctica. Cambridge University Press, Cambridge, pp. 83–87.
Hokada, T., Motoyoshi, Y., 2006. Electron microprobe technique for U–Th–Pb and REE chemistry of monazite, and its implications for pre-, peak- and post-metamorphic events of the Lützow-Holm Complex and the Napier Complex, East Antarctica. Polar Geoscience 19, 118–151.
Holland, T.J.B., Powell, R., 1998. An internally consistent thermodynamic data set for phases of petrological interest. Journal of Metamorphic Geology 16, 309–343.
Holland, T.J.B., Powell, R., 2003. Activity–composition relations for phases in petrological calculations: an asymmetric multicomponent formulation. Contributions to Mineralogy and Petrology 145, 492–501.
Holland, T.J.B., Powell, R., 2011. An improved and extended internally consistent thermodynamic dataset for phases of petrological interest, involving a new equation of state for solids. Journal of Metamorphic Geology 29, 333–383.
Iwamura, S., Tsunogae, T., Kato, M., Koizumi, T., Dunkley, D.J., 2013. Petrology and phase equilibrium modeling of spinel–sapphirine-bearing mafic granulite from Akarui Point, Lützow-Holm Complex, East Antarctica: implications for the *P–T* path. Journal of Mineralogical and Petrological Sciences 108, 345–350.
Kawakami, T., Hokada, T., Sakata, S., Hirata, T., 2016. Possible polymetamorphism and brine infiltration recorded in the garnet–sillimanite gneiss, Skallevikshalsen, Lützow-Holm Complex, East Antarctica. Journal of Mineralogical and Petrological Sciences 111, 129–143.
Kawakami, T., Higashino, F., Skrzypek, E., Satish-Kumar, M., Grantham, G., Tsuchiya, N., Ishikawa, M., Sakata, S., Hirata, T., 2017. Prograde infiltration of Cl-rich fluid into the granulitic continental crust from a collision zone in East Antarctica (Perlebandet, Sør Rondane Mountains). Lithos 274–275, 73–92.
Kawasaki, T., Ishikawa, M., Motoyoshi, Y., 1993. A preliminary report on cordierite-bearing assemblages from Rundvågshetta, Lützow-Holm Bay, East Antarctica: evidence for a decompressional *P–T* path? Proceedings of the NIPR Symposium on Antarctic Geosciences 6, 47–56.
Kawasaki, T., Nakano, N., Osanai, Y., 2011. Osumilite and a spinel + quartz association in garnet–sillimanite gneiss from Rundvågshetta, Lützow-Holm Complex, East Antarctica. Gondwana Research 19, 430–445.
Kazami, S., Tsunogae, T., Santosh, M., Tsutsumi, Y., Takamura, Y., 2016. Petrology, geochemistry and zircon U–Pb geochronology of a layered igneous complex from Akarui Point in the Lützow-Holm Complex, East Antarctica: implications for Antarctica–Sri Lanka correlation. Journal of Asian Earth Sciences 130, 206–222.
Kretz, R., 1983. Symbols for rock-forming minerals. American Mineralogist 68, 277–279.
Le Breton, N., Thompson, A.B., 1988. Fluid-absent (dehydration) melting of biotite in metapelites in the early stage of crustal anatexis. Contributions to Mineralogy and Petrology 99, 226–237.
Lee, H.Y., Ganguly, J., 1988. Equilibrium compositions of coexisting garnet and orthopyroxene: experimental determinations in the system FeO–MgO–Al_2O_3–SiO_2, and applications. Journal of Petrology 29, 93–113.
Moecher, D.P., Essene, E.J., Anovitz, L.M., 1988. Calculation and application of clinopyroxene–garnet–plagioclase–quartz geobarometers. Contribution to Mineralogy and Petrology 100, 92–106.
Motoyoshi, Y., Ishikawa, M., 1997. Metamorphic and structural evolution of granulites from Rundvågshetta, Lützow-Holm Complex, East Antarctica. In: Ricci, C.A. (Ed.), The Antarctic Region: Geological Evolution and Processes. Siena, Terra Antarctica, pp. 65–72.
Motoyoshi, Y., Matsubara, S., Matsueda, H., Matsumoto, Y., 1985. Garnet–sillimanite Gneiss from the Lützow-Holm Complex, East Antarctica. In: Memoirs of National Institute of Polar Research, Special Issue 37, pp. 82–94.
Motoyoshi, Y., Matsueda, H., Matsubara, S., Sasaki, K., Moriwaki, K., 1986. Explanatory Text of Geological Map of Rundvågskollane and Rundvågshetta, Antarctica. In: Antarctic Geological Map Series 24. National Institute of Polar Research, Japan.
Newton, R.C., Manning, C.E., 2007. Solubility of grossular, $Ca_3Al_2Si_3O_{12}$, in H_2O–NaCl solutions at 800 °C and 10 kbar, and the stability of garnet in the system $CaSiO_2$–Al_2O_3–H_2O–NaCl. Geochimica et Cosmochimica Acta 71, 5191–5202.
Newton, R.C., Manning, C.E., 2008. Solubility of corundum in the system Al_2O_3–SiO_2–H_2O–NaCl at 800 °C and 10 kbar. Chemical Geology 249, 250–261.
Newton, R.C., Smith, J.V., Windley, B.F., 1980. Carbonic metamorphism, granulites and crustal growth. Nature 288, 45–50.
Newton, R.C., Aranovich, L.Ya, Hansen, E.C., Vandenheuvel, B.A., 1998. Hypersaline fluids in Precambrian deep-crustal metamorphism. Precambrian Research 91, 41–63.
Newton, R.C., Touret, J.L.R., Aranovich, L.Y., 2014. Fluids and H_2O activity at the onset of granulite facies metamorphism. Precambrian Research 253, 17–25.
Nishimiya, Y., Tsunogae, T., Santosh, M., 2010. Sapphirine + quartz corona around magnesian (X_{Mg} ~0.58) staurolite from the Palghat-Cauvery Suture Zone, southern India: evidence for high-pressure and ultrahigh-temperature metamorphism within the Gondwana suture. Lithos 114, 490–502.
Nogi, Y., Jokat, W., Kitada, K., Steinhage, D., 2013. Geological structures inferred from airborne geophysical surveys around Lützow–Holm Bay, East Antarctica. Precambrian Research 234, 279–287.
Ohyama, H., Tsunogae, T., Santosh, M., 2008a. CO_2-rich fluid inclusions in staurolite and associated minerals in a high-pressure ultrahigh-temperature granulite from the Gondwana suture in southern India. Lithos 101, 177–190.
Ohyama, H., Tsunogae, T., Santosh, M., 2008b. Carbonic fluid inclusions in ultrahigh-temperature granulite from Kumiloothu in the northern Madurai Block, southern India. Journal of Mineralogical and Petrological Sciences 103, 273–278.
Perkins, D., Newton, R.C., 1981. Charnockite geobarometers based on coexisting garnet–pyroxene–plagioclase–quartz. Nature 292, 144–146.
Powell, R., Holland, T.J.B., 1988. An internally consistent thermodynamic dataset with uncertainties and correlations: 3. Application, methods, worked examples and a computer program. Journal of Metamorphic Geology 6, 173–204.
Roedder, E., 1984. Fluid inclusions. Review in Mineralogy, Mineralogical Society of America 12, 644.
Rosenberg, P.E., Foit Jr., F.F., 1977. Fe^{2+}-F avoidance in silicates. Geochimica et Cosmochimica Acta 41, 345–346.
Santosh, M., Omori, S., 2008. CO_2 flushing: a plate tectonic perspective. Gondwana Research 13, 86–102.
Santosh, M., Tsunogae, T., 2003. Extremely high density pure CO_2 fluid inclusions in a garnet granulite from Southern India. The Journal of Geology 111, 1–16.
Santosh, M., Yoshida, M., 1992. A petrologic and fluid inclusion study of charnockites from the Lützow-Holm Bay region, East Antarctica: evidence for fluid-rich metamorphism in the lower crust. Lithos 29, 107–126.
Santosh, M., Harris, N.B.W., Jackson, D.H., Mattey, D.P., 1990. Dehydration and incipient charnockite formation: a phase equilibria and fluid inclusion study from South India. The Journal of Geology 98, 915–926.
Santosh, M., Tsunogae, T., Ohyama, H., Sato, K., Li, J.H., Liu, S.J., 2008. Carbonic metamorphism at ultrahigh-temperatures: evidence from North China Craton. Earth and Planetary Science Letters 266, 149–165.
Santosh, M., Maruyama, S., Omori, S., 2009. A fluid factory in solid Earth. Lithosphere 1, 29–33.

Santosh, M., Tsunogae, T., Shimizu, H., Dubessy, J., 2010. Fluid characteristics of retrogressed eclogites and mafic granulites from the Cambrian Gondwana suture zone in southern India. Contributions to Mineralogy and Petrology 159, 349–369.
Satish-Kumar, M., Hermann, J., Tsunogae, T., Osanai, Y., 2006. Carbonation of Cl-rich scapolite boudins in Skallen, East Antarctica: evidence for changing fluid condition in the continental crust. Journal of Metamorphic Geology 24, 241–261.
Shiraishi, K., Yoshida, M., 1987. Explanatory Text of Geological Map of Botnneset, Antarctica. In: Antarctic Geological Map Series, Sheet 25. National Institute of Polar Research, Tokyo, p. 9.
Shiraishi, K., Hiroi, Y., Motoyoshi, Y., 1989. 1:250,000 Geological Map of Lützow-Holm Bay. National Institute of Polar Research, Tokyo.
Shiraishi, K., Ellis, D.J., Hiroi, Y., Fanning, C.M., Motoyoshi, Y., Nakai, Y., 1994. Cambrian orogenic belt in east Antarctica and Sri Lanka: implications for Gondwana assembly. The Journal of Geology 102, 47–65.
Shiraishi, K., Hokada, T., Fanning, C.M., Misawa, K., Motoyoshi, Y., 2003. Timing of thermal events in eastern Dronning Maud Land, East Antarctica. Polar Geoscience 16, 76–99.
Shiraishi, K., Dunkley, D.J., Hokada, T., Fanning, C.M., Kagami, H., Hamamoto, T., 2008. Geochronological Constraints on the Late Proterozoic to Cambrian Crustal Evolution of Eastern Dronning Maud Land, East Antarctica: a Synthesis of SHRIMP U–Pb Age and Nd Model Age Data. In: Geological Society, London, Special Publications, vol. 308, pp. 21–67.
Stevens, G., Clemens, J.D., 1993. Fluid-absent melting and the roles of fluids in the lithosphere: a slanted summary? Chemical Geology 108, 1–17.
Suda, Y., Kawano, Y., Yaxley, G., Korenaga, H., Hiroi, Y., 2008. Magmatic Evolution and Tectonic Setting of Metabasites from Lützow-Holm Complex, East Antarctica. In: Geological Society, London, Special Publications, vol. 308, pp. 211–233.
Takahashi, K., Tsunogae, T., 2017. Carbonic fluid inclusions in a garnet-pyroxene granulite from Austhovde in the Lützow-Holm Complex, East Antarctica: implications for a decompressional *P–T* path. Journal of Mineralogical and Petrological Sciences 112, 132–137.
Takahashi, K., Tsunogae, T., Santosh, M., Takamura, Y., Tsutsumi, Y., 2018. Paleoproterozoic (ca. 1.8 Ga) arc magmatism in the Lützow-Holm Complex, East Antarctica: implications for crustal growth and terrane assembly in erstwhile Gondwana fragments. Journal of Asian Earth Sciences 157, 245–268. https://doi.org/10.1016/j.jseaes.2017.07.053.
Takamura, Y., Tsunogae, T., Santosh, M., Tsutsumi, Y., 2018. Detrital zircon geochronology of the Lützow-Holm Complex, East Antarctica: implications for Antarctica–Sri Lanka correlation. Geoscience Frontiers 9 (2), 355–375.
Touret, J.L.R., 1985. Fluid regime in Southern Norway: the record of fluid inclusions. In: Tobi, A.C., Touret, J.L.R. (Eds.), The Deep Proterozoic Crust in the North Atlantic Provinces. Reidel, Dordrecht, pp. 517–549.
Touret, J.L.R., 2001. Fluids in metamorphic rocks. Lithos 55, 1–26.
Touret, J.L.R., Huizenga, J.M., 2011. Fluids in granulites. Geological Society of America Memoir 207, 25–37.
Touret, J.L.R., Huizenga, J.M., 2012. Fluid-assisted granulite metamorphism: a continental journey. Gondwana Research 21, 224–235.
Toyoshima, T., 2017. Geological Structures, Crustal Units, and Tectonics of the Lützow-Holm Complex, East Antarctica. Abstract of the 8th Symposium on Polar Science (NIPR, Japan), OGp9.
Tsunogae, T., Santosh, M., 2011. Fluids in high- to ultrahigh-temperature metamorphism along collisional sutures: record from fluid inclusions. Journal of Asian Earth Sciences 42, 330–340.
Tsunogae, T., van Reenen, D.D., 2007. Carbonic fluid inclusions in sapphirine + quartz bearing garnet granulite from the Limpopo Belt, southern Africa. Journal of Mineralogical and Petrological Sciences 102, 57–60.
Tsunogae, T., van Reenen, D.D., 2011. High-pressure and ultrahigh-temperature granulite-facies metamorphism of Precambrian high-grade terranes: case study of the Limpopo Complex. Geological Society of America Memoir 207, 107–124.
Tsunogae, T., van Reenen, D.D., 2014. High- to ultrahigh-temperature metasomatism related to brine infiltration in the Neoarchean Limpopo Complex: petrology and phase equilibrium modelling. Precambrian Research 253, 157–170.
Tsunogae, T., Santosh, M., Osanai, Y., Owada, M., Toyoshima, T., Hokada, T., 2002. Very high-density carbonic fluid inclusions in sapphirine-bearing granulites from Tonagh Island in the Archean Napier Complex, East Antarctica: implications for CO_2 infiltration during ultrahigh-temperature (T>1100°C) metamorphism. Contributions to Mineralogy and Petrology 143, 279–299.
Tsunogae, T., Osanai, Y., Owada, M., Toyoshima, T., Hokada, T., Crowe, W.A., 2003. High fluorine pargasites in ultrahigh temperature granulites from Tonagh Island in the Archean Napier Complex, East Antarctica. Lithos 70, 21–38.
Tsunogae, T., Santosh, M., Dubessy, J., 2008. Fluid characteristics of high- to ultrahigh-temperature metamorphism in southern India: a quantitative Raman spectroscopic study. Precambrian Research 162, 198–211.
Tsunogae, T., Dunkley, D.J., Horie, K., Endo, T., Miyamoto, T., Kato, M., 2014. Petrology and SHRIMP zircon geochronology of granulites from Vesleknausen, Lützow-Holm Complex, East Antarctica: Neoarchean magmatism and Neoproterozoic high-grade metamorphism. Geoscience Frontiers 5, 167–182.
Tsunogae, T., Yang, Q.Y., Santosh, M., 2015. Early Neoproterozoic arc magmatism in the Lützow-Holm Complex, East Antarctica: petrology, geochemistry, zircon U–Pb geochronology and Lu–Hf isotopes and tectonic implications. Precambrian Research 266, 467–489.
Tsunogae, T., Yang, Q.Y., Santosh, M., 2016. Neoarchean–Early Paleoproterozoic and Early Neoproterozoic arc magmatism in the Lützow-Holm Complex, East Antarctica: insights from petrology, geochemistry, zircon U–Pb geochronology and Lu–Hf isotopes. Lithos 263, 239–256.
Van den Kerkhof, A.M., Hein, U.F., 2001. Fluid inclusion petrography. Lithos 55, 27–47.
White, R.W., Powell, R., Holland, T.J.B., Worley, B.A., 2000. The effect of TiO_2 and Fe_2O_3 on metapelitic assemblages at greenschist and amphibolite facies conditions: mineral equilibria calculations in the system K_2O–FeO–MgO–Al_2O_3–SiO_2–H_2O–TiO_2–Fe_2O_3. Journal of Metamorphic Geology 18, 497–511.
White, R.W., Powell, R., Holland, T.J.B., Johnson, T.E., Green, E.C.R., 2014. New mineral activity–composition relations for thermodynamic calculations in metapelitic systems. Journal of Metamorphic Geology 32, 261–286.
Yoshimura, Y., Motoyoshi, M., Miyamoto, T., 2008. Sapphirine + Quartz Association in Garnet: Implication for Ultrahigh-temperature Metamorphism at Rundvågshetta, Lützow-Holm Complex, East Antarctica. In: Geological Society, London, Special Publications, vol. 308, pp. 377–390.